Oxid Met (2014) 81:467–476
DOI 10.1007/s11085-013-9458-z

ORIGINAL PAPER

Cyclic Oxidation Behavior of the Ti–6Al–4V Alloy

Shangwu Zeng · Aimin Zhao · Haitao Jiang · Xiang Fan · Xiaoge Duan · Xiaoqian Yan

Received: 22 September 2013 / Revised: 15 October 2013 / Published online: 29 October 2013

Abstract The cyclic oxidation behavior of the Ti–6Al–4V alloy has been studied under heating and cooling conditions within a temperature range from 550 to 850 °C in air for up to 12 cycles. The mass changes, phase, surface morphologies, cross-sectional morphologies and element distribution of the oxide scales after cyclic oxidation were investigated using electronic microbalance, X-ray diffractometry, scanning electron microscopy and energy dispersive spectroscopy. The results show that the rate of oxidation was close to zero at 550 °C, obeyed parabolic and linear law at 650 and 850 °C, respectively, while at 750 °C, parabolic—linear law dominated. The double oxide scales formed on surface of the Ti–6Al–4V alloy consisted of an inner layer of TiO_2 and an outer layer of Al_2O_3, and the thickness of oxide scales increased with an increasing oxidation temperature. At 750 and 850 °C, the cyclic oxidation resistance deteriorated owing to the formation of voids, cracks and the spallation of the oxide scales.

Keywords Ti–6Al–4V alloy · Cyclic oxidation · Oxidation kinetics · Oxide scales

Introduction

Titanium alloys are used for a wide variety of aviation aerospace, marine, chemical automotive industries because of their high specific strength and excellent corrosion

S. Zeng · A. Zhao · H. Jiang (✉) · X. Fan · X. Duan · X. Yan
Engineering Research Institute, University of Science and Technology Beijing, Beijing 100083, China
e-mail: nwpujht@163.com

S. Zeng · A. Zhao
Beijing Lab for Modern Transportation Metal Material and Processing Technology, Beijing 100083, China

resistance [1–5]. One of the most commonly used titanium alloys is an alpha–beta alloy containing 6 % Al and 4 % V. This alloy usually referred to as Ti–6Al–4V, and long working temperature up to 400 °C [6]. Therefore, the disks and blades of the first 4–5 stages of the compressor (low-pressure compressor) and static components can be made from Ti–6Al–4V [1, 4, 6]. However, the high temperature capability of the alloys is often limited by relatively poor resistance against hot gas. The high temperature oxidation products results in a loss of the load-bearing cross section and may be eventually limit the time at operating temperature to maintain integrity of the component. In addition, high oxygen solubility of titanium alloys results in a brittle oxygen-rich layer beneath the oxide scale during high temperature exposure and therefore decreases the plasticity significantly [4, 7–10]. Both modes of degradation, reaction product formation and embrittlement, require specific attention for component design and usage. High temperature exposure can limit the lifetime of a component and, like mechanical properties, must be considered carefully.

In literature [11–15], the isothermal oxidation behavior of Ti–6Al–4V alloy has been studied extensively and systematically. Guleryuz [12] found that the isothermal oxidation of Ti–6Al–4V followed parabolic kinetics between 600 and 700 °C and linear kinetics above 700 °C, the surfaces were mainly covered by anatase and rutile modification of TiO_2. The results from Wei [13] concerning on the isothermal oxidation of Ti–6Al–4V revealed all the involved elements diffused either outwardly or inwardly, depending on the concentration gradients. The substrate elements Ti and Al diffused outwardly toward the oxide/gas interface and the oxygen from the atmosphere diffused inwardly during oxidation. Alloys used at high temperature are subjected to duty cycles which vary widely among applications. The cyclic oxidation resistance is of the same importance as the isothermal oxidation resistance, as the thermal shock phenomenon frequently occurs in real applications, resulting in scales cracking and spalling when subject to thermal cycling, and consequently losing productivity. However, the cyclic oxidation of Ti–6Al–4V alloy, has not been investigated as extensively and systematically as the isothermal oxidation.

In order to fully understand of the cyclic oxidation behavior of Ti–6Al–4V alloy. In this paper, the cyclic oxidation behavior of Ti–6Al–4V was investigated at 550–850 °C in air up to 12 thermal cycles. The mass changes, phase, surface morphology, cross-sectional morphology, characteristics and element distribution of the oxide scales, and alpha case were discussed.

Experimental Procedures

Specimens of Ti–6Al–4V alloy were prepared by forging. The chemical composition of the specimens used in this experiment is shown in Table 1.

Specimens for cyclic oxidation tests were firstly cut with a size of $4 \times 12 \times 12$ mm^3. Then, all surfaces were ground with SiC waterproof paper to a final grade of 1,500 grit, and followed by ultrasonically cleaning in acetone and alcohol, respectively. The cyclic oxidation experiments were performed using a

Table 1 The chemical composition of the Ti–6Al–4V alloy/wt%

Ti	Al	V	Fe	C	N	H	O
Balance	6.390	4.120	0.160	0.008	0.009	0.005	0.160

muffle furnace (SRJX-4-13 Mode) at 550–850 °C in air for up to 12 thermal cycles. The specimens were then placed in an alumina crucible for quickly taking out and returning to ensure rapid heating and cooling. Each cycle of the oxidation experiment was composed of heating for 1 h in the muffle furnace at the setting temperature and cooling in air for 10 min. After 10 min cooling in air, and then of specimens the weight gain (crucible with specimen) and spallation (crucible without the specimen) were weighed by an electronic microbalance (AL204-IC Mode) with an accuracy of $\pm 10^{-4}$ g. The mass change value is the measurement of the average value of two specimens for each oxidation condition, and the oxidation kinetics curves were plotted using the average mass change.

The surface and cross-section morphologies of the oxide scales were performed using scanning electron microscopy (Zeiss, Ultra 55). Chemical composition and element profiles of scales were measures using energy-dispersive X-ray spectroscopy (Zeiss, Ultra 55). The scanning electron microscope with field emission gun was operated at 10 kV in InLens mode (surface morphologies) and 15 kV in AsB mode (cross-section morphologies). EDS analyses were carried out at an operation voltage of 10 kV using an Oxford Si detector. Oxidation products were identified with X-ray diffraction (TTRIII). The XRD was carried out under Cu Kα radiation, and the diffraction angle range was between 10° and 90° with a step increment of 0.02°. The alpha case was observed by optical microscope (ZEISS Axiovert 40MAT).

Results

Oxidation Kinetics

Figure 1 shows the mass change per unit surface area as a function of cyclic oxidation number at 550, 650, 750 and 850 °C in air. The displayed mass changes include the mass gain due to oxidation and the mass losses due to scale spallation. At 550 °C, the mass change were almost nil, indicating excellent resistance, without scale spallation, owing to the formation of thin, protective oxide scales. At 650 °C, mass gains were continuously measured after six cycles, but the mass changes have been small with the increase of the number of cyclic oxidation. At 750 °C, mass gains occur within four cycles, followed by small spalled oxide mass due to partial scale spallation, and large mass gains due to partial scale spallation cause the rate of scaling is fast. At 850 °C, bigger spalled oxide mass occur, because remarkable breakage and massive peeling off were observed on edges and the surface of the Ti–6Al–4V alloy after cycles oxidation. The mass gain of alloy kept monotonously increasing, suggesting that the mass gain due to oxidation is larger than the mass loss due to spallation.

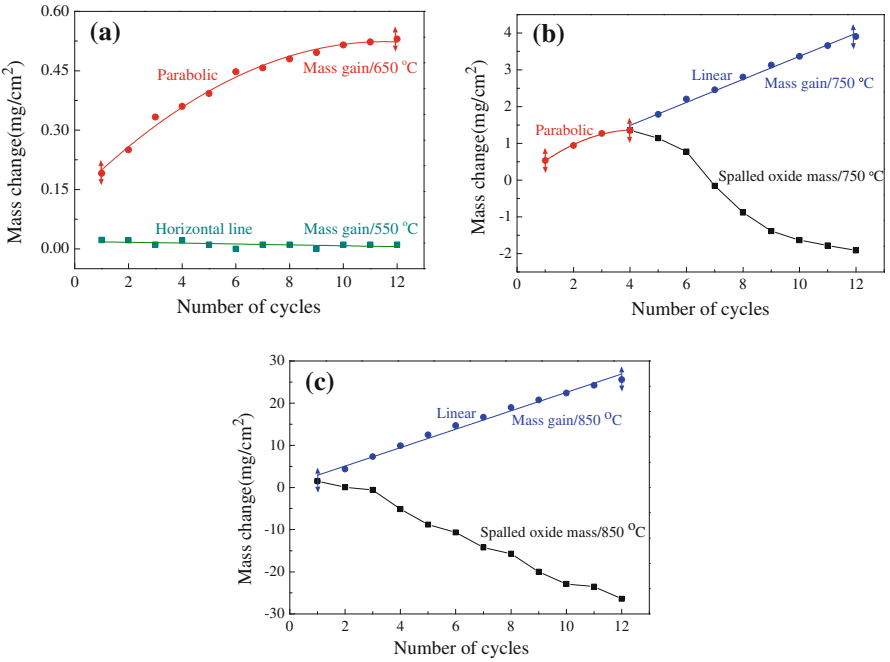

Fig. 1 Mass change versus oxidation number of Ti–6Al–4V alloy after 12 cycles oxidation at different temperature **a** 550 and 650; **b** 750; **c** 850 °C

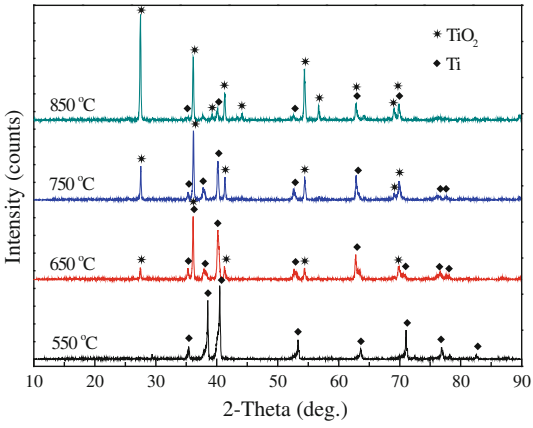

Fig. 2 X-ray diffraction patterns of Ti–6Al–4V alloy after 12 cycles oxidation at different temperature

Phase Detection of the Oxide Scale

The oxides formed of Ti–6Al–4V alloy at 550–850 °C after 12 thermal cycles were identified by XRD, as shown in Fig. 2. The surfaces were mainly covered by α-Ti and/or rutile modification of TiO_2. After cyclic oxidation at relatively low temperatures, i.e. at 550 °C, the characteristic diffraction peaks of α-Ti be detected only, which indicates the scale is very thin and a protective barrier has formed on

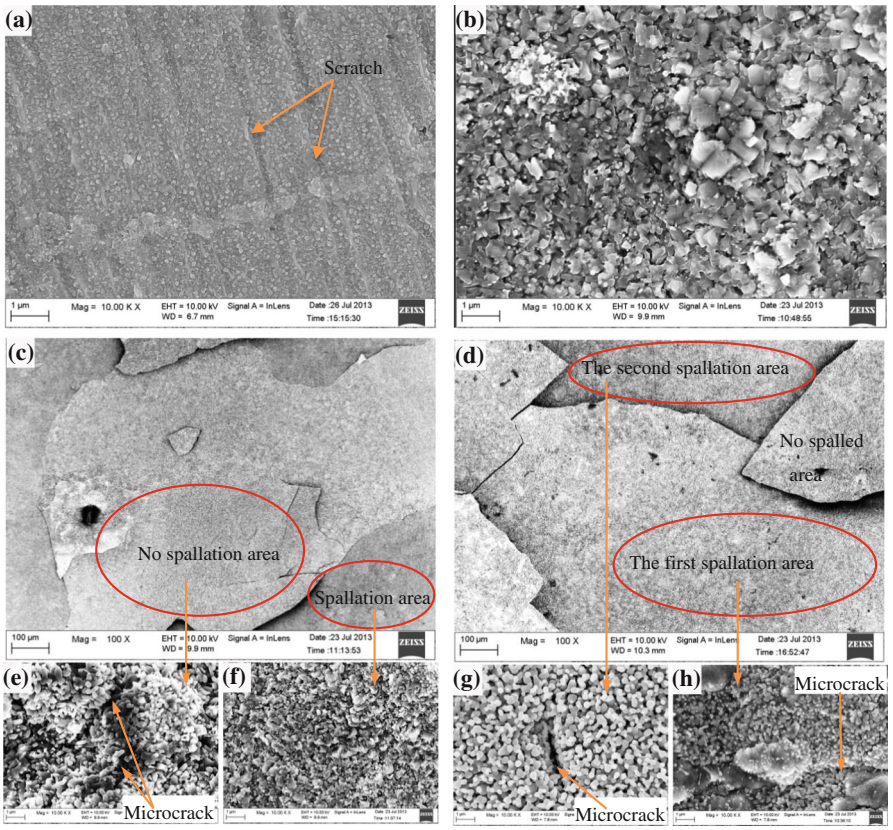

Fig. 3 SEM images of sample's surface morphologies after 12 cycles oxidation at different temperature **a** 550; **b** 650; **c** 750; **d** 850 °C; **e** no spallation area of (**c**); **f** spallation area of (**c**); **g** the second spallation area of **d**; **h** the first spallation area of (**d**)

the TiO_2 surface to reduce its further oxidation. With temperature increasing, α-Ti peak intensities were greatly reduced and TiO_2 peak intensities were greatly increased, which suggests the scale is gradually increasing.

Surface Morphology

Figure 3 shows the typical surface morphology of the oxide scales formed at different temperatures after 12 thermal cycles. At 550 °C, neither microcracks nor pores were observed, only small white point and scratch due to the polish of fabricating sample were observed to embed in the scale here (Fig. 3a). There were no scale cracks on surface at 650 °C, only some pores were observed in Fig. 3b. It is also well revealed that the surface of the scale consists of coarse and fine polygonal particles. At 750 °C, it's found such characteristic as obvious cracks and spalls on the surface, there are lots of dense "mushroom-shape" particles products in the spalled area, but, there are columnar shape particles scattered over the surface and

microcrack in the no spalled area, as shown in Fig. 3e, f, respectively. With increasing temperature, both span of the oxide scale cracks and number of the spalled increased (Fig. 3d), and the first spalled and second spalled layer were observed. There are white balls and pores on the second spalled surface (Fig. 3g). The scaled are full of pores and microcracks in the first or no spalled area (Fig. 3h).

Cross-Sectional Morphology

Figure 4 shows the cross-sectional images and elemental line-scan profile of the Ti–6Al–4V alloy after cyclic oxidation at 550, 650, 750 and 850 °C, respectively. At 550 °C, the thin oxide scale was well adherent to the substrate, and no pore or crack was observed (Fig. 4a). At 650 °C, the oxide scale thickness was about 4 μm, and part of the oxide scale has already been cracked. The oxide scale is divided into two and three sections at 750 and 850 °C, respectively. Figure 4g shows the oxide scale corresponding to the first spalled, second spalled and no spalled area of the Fig. 3d, and the three sections have been isolated (namely mixed solution of epoxy resin and ethylenediamine flow into between the two scale layers when cold mosaic). From the elemental line-scan profile, two O-enrichment zones were observed in the oxidation zone, one is TiO_2 layer, the other one is Al_2O_3 layer. The titanium content distributes in gradient descent from substrate to oxide scale (namely Fig. 4h-II zone). In addition, there were Al-depletion and Al-enrichment in the outmost oxide scale (namely Fig. 4f-I zone). The SEM and EDS analysis suggested that the oxide scale is of layered structure, a duplex oxide scales consisting of an inner thick and loose layer of rutile-TiO_2 and an outer thin and compact layer of α-Al_2O_3.

Discussion

From the Fig. 3a shown that the density oxidation scale is formed on the surface of Ti–6Al–4V alloy at 550 °C, and the mass change was horizontal line, as shown in Fig. 1a. It is suggests that the density oxidation scale can hinder inward diffusion of oxygen and reduce its further oxidation. The parabolic law applies if the oxidation kinetics is governed by the diffusion of species through the scales [16]. As seen in Fig. 1, the oxidation kinetics approximately follow the parabolic law at 650 °C. It is important to point out that, 750 °C dominated parabolic kinetics at cyclic oxidation times shorter than 5 h and conformed linear kinetics at cyclic oxidation times longer than 5 h. However, there is another important factor that should be taken into account, and that is scale spallation. In such a case, the parabolic law is no longer valid for a given system, and the oxidation is governed by a mechanism, such as transport through pores, cracks, etc. During 750 °C cyclic oxidation, inward diffusion of oxygen is through oxide scales, then pores and/or cracks. In fact, the cyclic oxidation of Ti–6Al–4V alloy is governed by inward diffusion of oxygen through the pores and cracks of scales at 850 °C.

At the initial stages of oxidation, the TiO_2 scale formed by inward diffusion of oxygen on the surface of Ti–6Al–4V alloy, a titanium-depleted zone can form in the oxide/substrate interface as a result of scale forming titanium-depletion. It results in

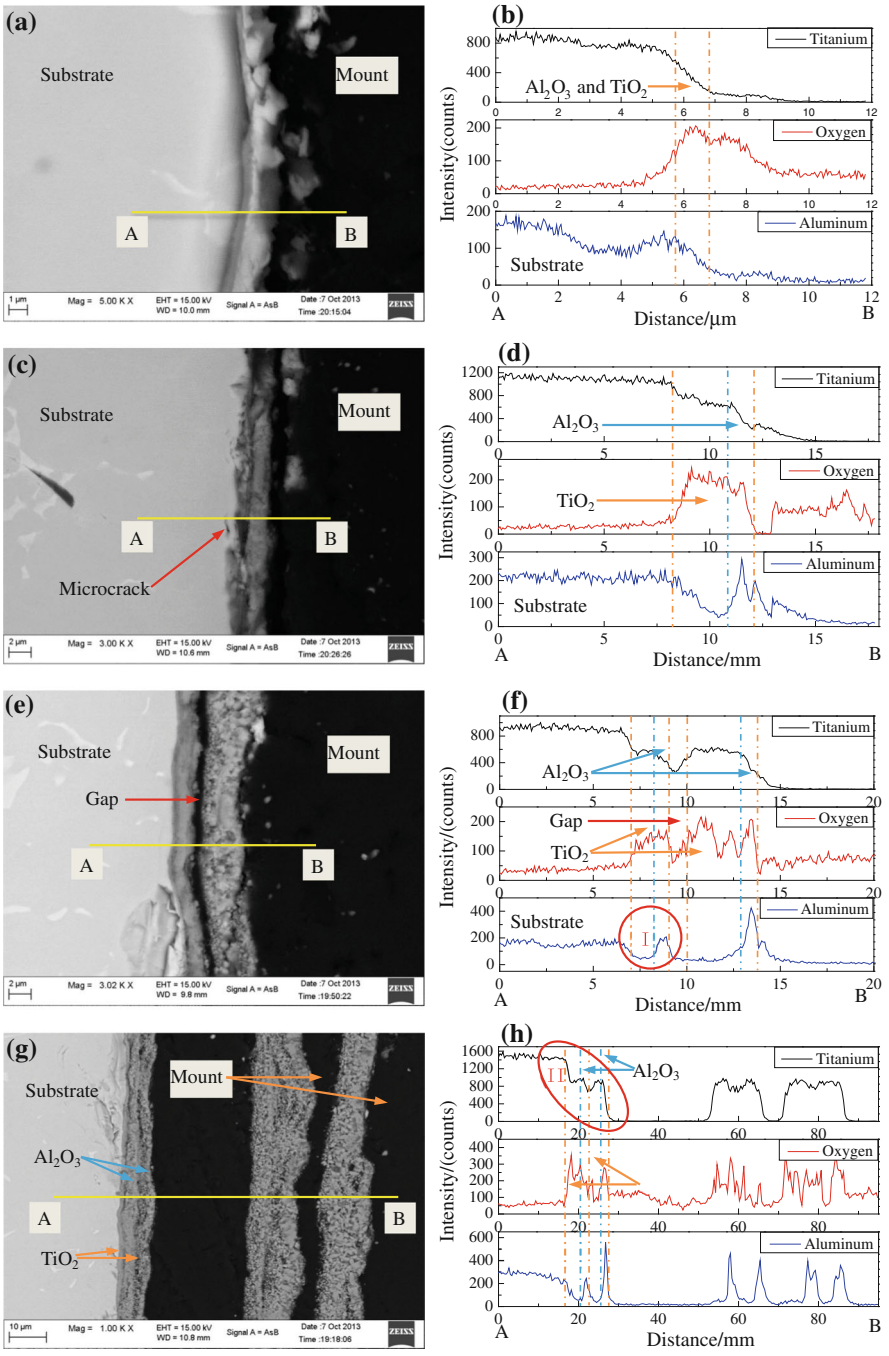

Fig. 4 The cross-sectional morphology and EDS analyses of the scale after 12 cycles oxidation at different temperature, **a** 550 °C; **b** line profiles across A and B of (**a**); **c** 650 °C; **d** line profiles across A and B of (**c**); **e** 750 °C; **f** line profiles across A and B of (**e**); **g** 850 °C; **h** line profiles across A and B of **g**

local enrichment of Al in the oxide/substrate interface, and leaded to outward diffused of aluminum from the oxide/substrate interface to the gas/oxide interface and form a thin Al_2O_3. As extended oxidation times, Al_2O_3 grows laterally and covers TiO_2. In this case, the outer most section of the oxidation layer is Al_2O_3 (though Al_2O_3 peaks were not appeared on the XRD patterns of this paper (Fig. 3), weak diffraction peaks of α-Al_2O_3 was detected after oxidation time of 100 h by Li [14]), while the inner section of the oxidation layer is TiO_2. Therefore, the formation of double layered oxide scales on the surface of Ti–6Al–4V alloy. The TiO_2 layer and Al_2O_3 layer grew alternately and thus producing a multilayered oxide scales, and it was particularly evident in the 850 °C, as shown in Fig. 4g. Until reaching a critical thickness, oxide layer maintains a good contact with the substrate. But cracks will form between the oxide scale and substrate once a critical thickness of the oxide scale is exceeded [15]. On the other hand, crack defect would promote inward diffuse of oxygen to the oxide/substrate interface and react with titanium to form TiO_2 and increase the thickness of the TiO_2 layer.

Under cyclic oxidation conditions, the stress formed during the oxidation process could be classified as two types. One is the growth stress, it is generated during oxidation by alloy to oxide volume expansion and/or the formation of oxide within the oxide scale. The growth stress results in compressive stress in the oxide scale and tensile stress in the substrate. The other one is the thermal stress formed during the cooling due to the mismatch of the thermal expansion coefficient between the oxide scale and the alloy. One reason for the spallation of the oxide scale is the mismatch of the thermal expansion coefficient between the oxide scale and the substrate during cooling. The thermal expansion coefficient of the TiO_2 is about $8.2 \times 10^{-6}(K^{-1})$ [17], α-Al_2O_3 is about $8.1 \times 10^{-6}(K^{-1})$ [18], while that of the Ti–6Al–4V alloy is about $10–12 \times 10^{-6}(K^{-1})$ [19]. Mismatch of the thermal expansion coefficient between the oxide scale and the Ti–6Al–4V alloy resulted in the formation of large compressive stresses in the oxide scale and then the spallation of the oxide scale during cooling. The larger the temperature change, the bigger the thermal stress. Hence, severe cracking and partial spallation of the scale occurred at 850 °C, as shown in Fig. 3d. Another reason may be that a hardened alpha case formed beneath the oxide scale due to the oxygen dissolution. The plasticity of the hardened alpha case is much lower than that of the substrate at high temperature, so the high growth stresses of the oxide scale may not be able to be released by the plastic flow of the substrate and probably result in the formation of the cracks. During the course of the experiment, it can be found that the source of crack is formed during the fast cooling process at 750 °C cyclic oxidation, however, the crack is formed during the fast heating or heat preservation process at 850 °C cyclic oxidation, and further enhances generation and expansion of cracks at the subsequent fast cooling stage. The number of spallation and size of cracks increased with the increase of the cycle oxidation number.

It can be seen from Fig. 5 that the growth of oxide scale on the surface of Ti–6Al–4V alloy is accompanied by development of oxygen diffusion zone due to the diffusion of oxygen beyond the oxide scale, pore and crack. The oxygen diffusion zone is known as “alpha case”. The depth of alpha case is low in the case of specimen exposed at 650 °C, more at 750 °C and, highest at 850 °C (no alpha case

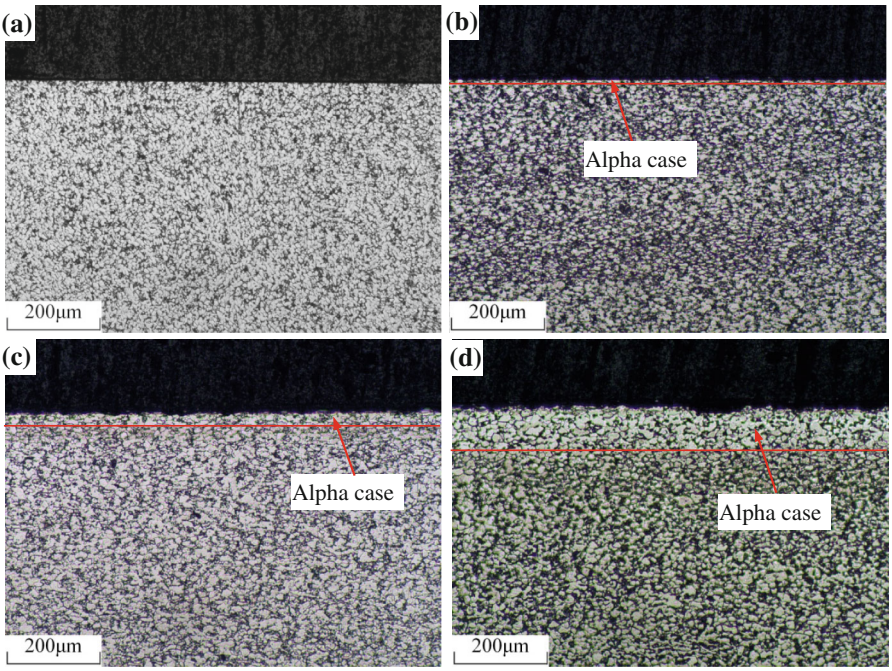

Fig. 5 Metallographic cross-sectional morphology of the scale after 12 cycles oxidation at different temperature, **a** 550; **b** 650; **c** 750; **d** 850 °C

at 550 °C). It indicates that alpha case formation is a diffusion controlled process, the depth of alpha case increases with increasing oxidation temperature. Since oxygen is α-Ti stabilizer [1] and peaks of β-Ti did not appear on the XRD pattern (Fig. 2), and oxygen rapidly diffuses through this oxide layer and dissolves in the substrate. Alpha case formation can substantially degrade the structural integrity of the affected titanium alloy by loss of tensile ductility and of fatigue resistance, even though the interior of the alloy is not subject to structural modification [4, 20]. So, alpha-case formation is critical to the life expectancy of titanium alloys when used in aero-gas turbine engines.

Conclusions

Cyclic oxidation of Ti–6Al–4V alloy followed parabolic and linear rate law at 650 and 850 °C, respectively. At 750 °C, oxidation of the alloy obeyed a parabolic rate law, and linear rate law after 5 h. There were no scale cracks in surface at 550 and 650 °C cyclic oxidation, and the oxide scale cracks and peels off were observed if the temperature is over 650 °C. Cyclic oxidation of Ti–6Al–4V alloy is governed by inward diffusion of oxygen through oxide scales and/or pores and cracks. The double oxide scales and alpha case formed on and below Ti–6Al–4 V alloy surface,

respectively, and the thickness of oxide scales and depth of alpha case increased with increasing temperature.

References

1. C. Leyens and M. Peters, *Titanium and Titanium Alloys, chapt. 1*, (Wiley-VCH, Weinheim, 2003).
2. V. N. Moiseyev, *Titanium Alloys: Russian Aircraft Aerospace Applications, chapter 6*, (Taylor & Florida Group: CRC, Boca Raton, 2006).
3. J. C. Williams, *Materials Science and Engineering A* **263**, 107 (1999).
4. R. R. Boyer, *Materials Science and Engineering A* **213**, 103 (1999).
5. I. Gurrappa, *Materials Characterization* **51**, 131 (2003).
6. China Aeronautical Materials Handbook Editorial Board, *China Aeronautical Materials Handbook*, Vol. 4 (China Standard Press, Beijing, 2002).
7. Y. Xiong, S. Zhu and F. Wang, *Surface and Coatings Technology* **190**, 195 (2005).
8. R. N. Shenoy, J. Unnam and R. K. Clark, *Oxidation of Metals* **26**, 105 (1986).
9. C. Leyens, M. Peters, D. Weinem and W. A. Kaysser, *Metallurgical and Materials Transactions A* **27A**, 1709 (1996).
10. I. Gurrappa and A. K. Gogia, *Surface and Coatings Technology* **139**, 216 (2001).
11. H. Lee, J. Yoon and Y. Yi, *Thermochimica Acta* **455**, 105 (2007).
12. H. Guleryuz and H. Cimenoglu, *Journal of Alloys and Compounds* **472**, 241 (2009).
13. D. Wei, P. Zhang, Z. Yao, W. Liang, Q. Miao and Z. Xu, *Corrosion Science* **66**, 43 (2013).
14. W. Li, S. Zhu, C. Wang, M. Chen, M. Shen and F. Wang, *Corrosion Science* **74**, 367 (2013).
15. H. L. Du, P. K. Datta, D. B. Lewis and J. S. Burnellgray, *Corrosion Science* **36**, 631 (1994).
16. D. Wei, P. Zhang, Z. Yao, J. Zhou, X. Wei and P. Zhou, *Applied Surface Science* **261**, 800 (2012).
17. S. S. Jiang and K. F. Zhang, *Materials & Design* **30**, 3904 (2009).
18. R. G. Munro, *Journal of the American Ceramic Society* **80**, 1919 (1997).
19. B. Huang, C. Li, L. Shi, G. Qiu and T. Zuo, *China Materials Engineering Canon, (vol. 4): Non-Ferrous Metal Materials Engineering*, (Chemical Industry Press, Beijing, 2006).
20. I. Gurrappa, *Journal of Alloys and Compounds* **389**, 190 (2005).